# LMK235, a small molecule inhibitor of HDAC4/5, protects dopaminergic neurons against neurotoxin- and α-synuclein-induced degeneration in cellular models of Parkinson's disease

Martina Mazzocchi [a], Susan R. Goulding [a], Sean L. Wyatt [b], Louise M. Collins [a,c], Aideen M. Sullivan [a,d,*], Gerard W. O'Keeffe [a,d,*]

[a] Department of Anatomy & Neuroscience, University College Cork (UCC), Cork, Ireland
[b] School of Biosciences, Cardiff University, Cardiff, United Kingdom
[c] Department of Physiology, UCC, Cork, Ireland
[d] APC Microbiome Ireland, UCC, Cork, Ireland

## ARTICLE INFO

## ABSTRACT

Epigenetic modifications in neurodegenerative disease are under investigation for their roles in disease progression. Alterations in acetylation rates of certain Parkinson's disease (PD)-linked genes have been associated with the pathological progression of this disorder. In light of this, and given the lack of disease-modifying therapies for PD, HDAC inhibitors (HDIs) are under consideration as potential pharmacological agents. The neuroprotective effects of pan-HDACs and some class-specific inhibitors have been tested in *in vivo* and *in vitro* models of PD, with varying outcomes. Here we used gene co-expression analysis to identify HDACs that are associated with human dopaminergic (DA) neuron development. We identified HDAC3, HDAC5, HDAC6 and HDAC9 as being highly correlated with the DA markers, *SLC6A3* and *NR4A2*. RT-qPCR revealed that mRNA expression of these HDACs exhibited similar temporal profiles during embryonic mouse midbrain DA (mDA) neuron development. We tested the neuroprotective potential of a number of class-specific small molecule HDIs on human SH-SY5Y cells, using neurite growth as a phenotypic readout of neurotrophic action. Neither the class I-specific HDIs, RGFP109 and RGFP966, nor the HDAC6 inhibitor ACY1215, had significant effects on neurite outgrowth. However, the class IIa HDI, LMK235 (a HDAC4/5 inhibitor), significantly increased histone acetylation and neurite outgrowth. We found that LMK235 increased BMP-Smad-dependent transcription in SH-SY5Y cells and that this was required for its neurite growth-promoting effects on SH-SY5Y cells and on DA neurons in primary cultures of embryonic day (E) 14 rat ventral mesencephalon (VM). These effects were also seen in SH-SY5Y cells transfected with HDAC5 siRNA. Furthermore, LMK235 treatment exerted neuroprotective effects against degeneration induced by the DA neurotoxin 1-methyl-4-phenylpyridinium (MPP$^+$), in both SH-SY5Y cells and cultured DA neurons. Treatment with LMK235 was also neuroprotective against axonal degeneration induced by overexpression of wild-type (WT) or A53T mutant α-synuclein in both SH-SY5Y cells and primary cultures of DA neurons. In summary, these data show the neuroprotective potential of the class IIa HDI, LMK235, in cell models of relevance to PD.

## 1. Introduction

Parkinson's disease (PD) is a common, progressive neurodegenerative disease (Poewe et al., 2017). While both genetic and environmental factors have been implicated in PD, the aetiology of the sporadic cases is not fully understood (Kalia and Lang, 2015). The progression of PD pathology is associated with loss of dopaminergic (DA) neurons in the midbrain of the substantia nigra (SN), and their projections to the striatum, accompanied by accumulation of intracellular inclusions of misfolded α-synuclein in Lewy bodies (Spillantini et al., 1997). The presence of these inclusions may alter several cellular mechanisms, including mitochondrial dynamics, axonal transport, microglial homeostasis and the ubiquitin proteasome system (Rocha et al., 2018). Post-mortem studies have shown that one year after PD diagnosis, 30% of SN DA neurons have been lost, with a 50–70% reduction in DA

---

---

**Abbreviations**

| | |
|---|---|
| α-syn | α-synuclein |
| AAV | adeno-associated virus |
| acH3-K9.K14 | histone acetylated lysine 9, lysine 14 |
| BMP | bone morphogenetic protein |
| BMPR1B | bone morphogenetic type 1 receptor |
| CaMK | $Ca^{2+}$/calmodulin-dependent protein kinase |
| DA | dopaminergic |
| DRG | dorsal root ganglion |
| HAT | histone acetyltransferase |
| HDAC | histone deacetylase |
| HDIs | HDAC inhibitors |
| iPSC | induced pluripotent stem cell |
| LDH | lactate dehydrogenase |
| mDA | midbrain DA |
| $MPP^+$ | 1-methyl-4-phenylpyridinium |
| MPTP | 1-methyl-4-phenyl-1,2,3,6-tetrahydropyridine |
| NaB | sodium butyrate |
| PD | Parkinson's disease |
| PINK1 | PTEN-induced putative kinase 1 |
| PKD | protein kinase D |
| shRNA | short hairpin RNA |
| siRNA | short interfering RNA |
| SN | substantia nigra |
| TH | tyrosine hydroxylase |
| VPA | valproic acid |

---

innervation of the striatum (Beach et al., 2008). This, along with evidence from several other studies, shows the importance of axonal degeneration as an early pathogenic event in the development of PD (O'Keeffe and Sullivan, 2018). A study by Chu et al. demonstrated dramatic decreases in axonal transporter proteins in α-synuclein-positive nigral neurons in samples from early-stage PD patients, suggesting that dysfunction of axonal transport has a critical role in the pathology of sporadic PD (Chu et al., 2012). Another study found that induced pluripotent stem cells (iPSCs) generated from a PD patient carrying the A53T α-synuclein mutation developed evidence of neurite degeneration, such as swollen varicosities and spheroid inclusions (Kouroupi et al., 2017). In addition to these effects on α-synuclein and axons, other alterations of epigenetic mechanisms have been found in PD models and may contribute to the pathogenesis of this disease (Labbe et al., 2016).

One key epigenetic mechanism is the process of histone acetylation. Histone acetylation is regulated by the action of two classes of enzymes, histone acetyltransferases (HATs) and histone deacetylases (HDACs), which regulate chromatin remodelling through the addition or removal of acetyl groups on histone tails, respectively (Kurdistani and Grunstein, 2003). PD patients have an abnormal pattern of histone acetylation in genes related to histone degradation, autophagy, aging and DNA repair mechanisms, when compared to controls (Mazzocchi et al., 2020; van Heesbeen and Smidt, 2019). Moreover, overexpression of nuclear-localised α-synuclein in the SH-SY5Y cell line promoted cell death that could be rescued by the administration of pan-HDAC inhibitors (Kontopoulos et al., 2006). That study also found that α-synuclein co-localises in the nucleus with histone 3, preventing its acetylation *in vivo* (Kontopoulos et al., 2006). These data suggest that an imbalance of HAT-HDAC homeostasis may be involved in the molecular pathology of PD (van Heesbeen and Smidt, 2019).

This evidence for dysregulation of histone acetylation in PD has led to the emergence of HDACs as potential drug targets. HDACs can be targeted by pharmaceutical agents called HDAC inhibitors (HDIs), which are classified as either pan-HDIs or inhibitors of specific classes of HDACs. There are four classes- Class I which includes the Zinc-dependent enzymes HDAC1, HDAC2, HDAC3 and HDAC8, Class IIa which includes HDAC4, HDAC5, HDAC7, HDAC9, Class IIb (HDAC6 and HDAC10), Class III (also called SIRT1-7), which are $NAD^+$ dependent enzymes, and Class IV which includes only HDAC11 (de Ruijter et al., 2003; Yang and Seto, 2007). Recently, studies have reported that treatment with pan-HDIs exacerbated 1-methyl-4-phenylpyridinium ($MPP^+$)-induced neurotoxicity in SH-SY5Y cells, whereas HAT activation promoted their survival (Choong et al., 2016; Hegarty et al., 2016a). HDIs have been examined as potential therapeutic agents for PD, however it is not yet clear which of the HDACs should be targeted for optimal therapeutic effect. Pharmacological inhibition of the Class I HDACs, namely HDAC1 and HDAC2, has been reported to attenuate $MPP^+$-induced toxicity in SH-SY5Y cells and 1-methyl-4-phenyl-1,2,3,6-tetrahydropyridine (MPTP)-induced death of DA neurons in mice *in vivo* (Choong et al., 2016). Others have shown that Tubastatin A and MS275, which block HDAC1 and HDAC2, ameliorated $MPP^+$-induced motor impairment in a zebrafish model of PD (Pinho et al., 2016). In contrast, Park et al. demonstrated that siRNA-mediated inhibition of HDAC1 and HDAC2 exacerbated $MPP^+$-induced death of SH-SY5Y cells, while overexpression of these Class I HATs was neuroprotective (Park et al., 2016). A role for HDAC3 in PD has been suggested by a study showing that PTEN-induced putative kinase 1 (PINK1) mutations, which are linked to autosomal recessive PD, can enhance the activity of HDAC3 in suppressing neuronal death *via* apoptosis (Choi et al., 2015). A role for Class II HDACs in PD has also been suggested from studies conducted on animal models. Cultured DA neurons from wild-type (WT) α-synuclein or A53T mutant α-synuclein transgenic mice, or from control transgenic mice treated with $MPP^+$, displayed increased DA neuronal death which was coupled with nuclear accumulation of HDAC4 *in vitro*; this was also confirmed *in vivo* in α-synuclein transgenic mice treated with MPTP (Wu et al., 2017). Other evidence for HDAC4 as a potential target for PD therapy came from a study on iPSC-derived dopamine neurons from a PD patient, which revealed that HDAC4 acted as a repressor of a set of 60 genes that were significantly upregulated or downregulated compared to age-matched controls (Lang et al., 2019). Another Class II HDAC, HDAC5, has been found to be upregulated in 80 distinct samples from 40 different brain regions of adult mice, following methamphetamine-induced neuronal death (Hourani et al., 2008). Inhibition of HDAC5 and HDAC9 has been reported to be neuroprotective in both $MPP^+$ and α-synuclein cell models of PD (Collins et al., 2015; Mazzocchi et al., 2019). Collectively, these studies suggest that upregulation and/or nuclear accumulation of class IIa HDACs may be detrimental to DA neurons. A role for the Class IIb HDAC, HDAC6, has been suggested by a study showing that HDAC6 overexpression can rescue misfolded protein accumulation that occurs as a result of autophagy activation in a Drosophila transgenic model of PD (Pandey et al., 2007).

Collectively, these studies suggest roles for various classes of HDACs in PD neuropathology; thus, it is important to identify which class is the most appropriate to target for neuroprotective therapy. In this study, we investigated the effects of several class-specific HDIs in two cell models of PD. We used neurite outgrowth as a phenotypic readout of the neurotrophic effects of these agents, since axonal degeneration is an early pathological event in PD.

## 2. Methods

### 2.1. Gene co-expression analysis of human SN

Human SN from healthy controls (GSE:60863) (Ramasamy et al., 2014) gene expression data were analysed using R2 Genomics Analysis and Visualization Platform[1]. Pearson correlation and Bonferroni

multiple comparison tests were used to assess which HDACs were significantly co-expressed with *SLC6A3* and *NR4A2* genes, two markers of DA neurons. All gene expression data are presented as log2 expression values.

## 2.2. Cell culture

The two cell models used in this work were SH-SY5Y cells (ATCC; CRL-2266) and primary cultures of embryonic day (E) 14 rat ventral mesencephalon (VM). The SH-SY5Y cell line is an extensively-used model of human DA neurons (Xicoy et al., 2017). These cells were grown in Dulbecco's Modified Eagle Medium Nutrient Mixture F-12 (DMEM/F-12), supplemented with 10% foetal bovine serum (FBS), 100 nM ʟ-Glutamine, 100 U/ml Penicillin, 10 μg/ml Streptomycin (all Sigma), in a humidified atmosphere containing 5% $CO_2$ at 37 °C. No differentiating agent was applied, since SH-SY5Y cells develop clear neurites when cultured at low density and the use of a differentiating agent can cause them to be less susceptible to the effects of MPP+ (Cheung et al., 2009). Primary cultures of E14 rat VM (from the Biological Service Unit, University College Cork) were prepared as previously described (Hegarty et al., 2016c) under license with full ethical approval. After dissection, the VM tissue was dissociated following enzymatic treatment and cells were plated in poly-ᴅ-lysine-coated 24-well plates (Sigma) in DMEM/F-12 media supplemented with 1% penicillin/streptomycin (Sigma), 1% ʟ-glutamine (Sigma), 2% B27 (Invitrogen) and 1% FBS. Where indicated, cells were pre-treated for 30 min with 1 μg/ml of the bone morphogenetic type 1 receptor (BMPR1) inhibitor, dorsomorphin (Sigma), which is known to inhibit BMPR1B receptors (Yu et al., 2008). Class I HDIs, RGFP109, RGFP966, Class-IIa HDIs, LMK-235, TMP-269 and Class IIb HDI ACY1215 (Cayman) were added at concentrations ranging from 0.001–0.1 μM, as indicated in each figure, with or without 1 mM MPP+, a DA neurotoxin widely used as an *in vitro* PD model (Chun et al., 2001), or pre-treated with 1 μg/ml dorsomorphin for 30 min. Where indicated, E14 VM cultures were plated at a density of $1.0 \times 10^5$ cells per well of a 24-well plate and transduced with 4 μl AAV2/6-GFP or 3.84 μl of AAV2/6-α-Synuclein to achieve a multiplicity of infection (MOI) of $2.0 \times 10^5$. Cultures were then treated daily with 20 nM of LMK235, commencing 5 days after viral infection (delayed treatment). The experimental endpoint was 10 DIV.

## 2.3. Plasmid transfection

SH-SY5Y cells were transfected using the TransIT-X2® Dynamic Delivery System (Mirus Bio) according to the manufacturer's instructions. Briefly, SH-SY5Y cells were seeded at a density of $1.5 \times 10^5$ cells per well of a 24-well plate at 1 DIV. Where indicated, cells where transfected with 500 ng of pcDNA3-EGFP, a gift from Professor Doug Golenbock (Addgene plasmid # 13031; http://n2t.net/addgene:13031; RRID: Addgene_13031) or 500 ng of EGFP-alphasynuclein-wild-type (Addgene plasmid # 40822; http://n2t.net/addgene:40822; RRID: Addgene_40822) or 500 ng of EGFP-alphasynuclein-A53T (Addgene plasmid #40823; http://n2t.net/addgene:40823; RRID:Addgene_40823) both gifted by Prof. David Rubinsztein (Furlong et al., 2000). Where indicated, cells were also transfected with 500 ng of GFP Cignal reporter (Qiagen CCS-017G). Cells were subsequently treated with 0.1 μM of TMP269 or LMK235 for 72 h, or 1 μg/ml Dorsomorphin for 24 h. For siRNA experiments, cells were co-transfected with pcDNA3-EGFP and with 25 nM of commercially available *Silencer*® pre-designed siRNAs targeting *HDAC5* (siHDAC5) or scrambled control siRNA (siSCR) (ThermoFisher).

## 2.4. Virus preparation

Expression plasmids for α-synuclein and GFP were kindly gifted by Dr. Eilis Dowd (National University of Ireland, Galway) and Professor Deniz Kirik (Lund University, Sweden). Adeno-associated viral 2/6

vectors (AAV) were generated by Vector Biosystems Inc. (Philadelphia, USA), driven by a synapsin-1 promoter and enhanced using a woodchuck hepatitis virus post-transcriptional regulatory element (WPRE). The final viral titres for AAV2/6-α-synuclein and AAV2/6-GFP were $5.2 \times 10^{13}$ gc/ml and $5.0 \times 10^{13}$ gc/ml, respectively.

## 2.5. Immunocytochemistry, cell labelling and analysis of neurite growth

To image SH-SY5Y cells for neurite length analysis, cells were fluorescently labelled by incubation in the vital dye calcein AM (1:1000 Invitrogen) for 1 h at the end of the three-day culture period. For primary cultures, DA neurons were identified by immunocytochemical staining for TH. Cell culture plates were fixed for 15 min using 4% paraformaldehyde. Following $3 \times 5$ min washes in 10 mM phosphate-buffered saline – Triton X-100 (PBS-T) (0.02% Triton X-100 in 10 mM PBS), cultures were incubated in 5% bovine serum albumin (BSA) in 10 mM PBS-T for 1 h at room temperature. They were subsequently incubated with the following primary antibodies: TH (Millipore MAB318; 1:200); α-synuclein (Millipore 36/008; 1:2000); Smad1/5/9 (Abcam ab66737; 1:200); phospho-Smad 1/5/9 (Cell Signalling 13820S; 1:200) or AcH3 K9-K14 (Santa Cruz sc-33361; 1:200), diluted in 1% BSA in 10 mM PBS at 4 °C for 16 h. Following $3 \times 5$ min washes in 10 mM PBS-T, cultures were incubated in 594-conjugated Alexa-Fluor® secondary antibodies (Invitrogen; 1:500 A11005 or A11012) in 1% BSA in 10 mM PBS prior to $3 \times 5$ min washes. All stained cultures of SH-SY5Y cells and of E14 VM neurons were imaged using an Olympus IX71 inverted microscope. For analysis of neurite growth in all cultures, five non-overlapping images were captured from each well in each experimental group and 135–350 cells were analysed per group, as indicated in the figure legends. Neurite growth was measured by opening each image in Image J, and manually tracing the length of a given neurite using the trace function in Image J. Where indicated, the fluorescence intensity of individual cells was measured by densitometry using Image J analysis software.

## 2.6. Quantitative real-time PCR (RT-qPCR)

The levels of *Hdac3*, *Hdac5*, *Hdac6* and *Hdac9* mRNAs in embryonic and neonatal DA neurons of mouse VM (E10-P1) were quantified by RT-qPCR relative to a geometric mean of mRNAs for the housekeeping enzymes, glyceraldehyde phosphate dehydrogenase (*Gapdh*), succinate dehydrogenase (*Sdha*) and hypoxanthine phosphoribosyltransferase-1 (*Hprt1*), as previously described (Hegarty et al., 2017). Briefly, 5 μl of RNA from the midbrain was reverse transcribed for 1 h at 45 °C using the AffinityScript kit (Agilent, Berkshire, United Kingdom) in a 25 μl reaction volume, following the manufacturer's instructions. 2 μl of cDNA was amplified in a 20 μl reaction volume using Brilliant III ultrafast qPCR master mix reagents (Agilent Technologies) with 150 nM of primers and 300 nM of dual-labelled (FAM/BHQ1) hybridization probes specific to each of the cDNAs (MWG/Eurofins, Ebersberg, Germany) using the Mx3000P platform (Agilent). The PCR primers were: *Hdac3* forward: 5′-GTG TCC TTC CAC AAA TAC-3′ and reverse: 5′-GCA CAT TGA GAC AAT AGT A-3′; *Hdac5* forward: 5′-TCC CTC CTA CAA ATT GCC-3 and reverse: 5′-GGT GAT CTC AAC TGC TCT C-3′; *Hdac6* forward: 5′-CTG ACT ACA TTG CTG CTT TC-3′ and reverse: 5′-CCA CCA AGA CCA GTT GAG-3′; *Hdac9* forward: 5′-CGT CTC CAT CCT ACA AGT A-3′ and reverse: 5′-CTC CTC TCT GCC ACT TTC-3′. Dual-labelled probes were: *Hdac3*: 5′-FAM-CCA CTC TCT GCT CCA ACT TCA TAC A-BHQ1-3′; *Hdac5*: 5′-FAM-CCC TAT GAC AGC CGT GAT GAC T-BHQ1-3′; *Hdac6*: 5′-FAM-CTG CCA GTT GCC TCG GAG TT-BHQ1-3′; *Hdac9*: 5′-FAM TAA CCT GGA CCG CAC CTT CAA BHQ1-3′.

## 2.7. LDH assay

The lactate dehydrogenase (LDH) colorimetric assay (Thermo Fisher) was used to determine the effects of different HDIs on toxicity/cell

viability. Briefly, cultures were treated with class-specific HDIs for 3 DIV and the culture medium was collected and centrifuged at 1000 rpm for 5 min at room temperature at the end of the three-day culture period. LDH activity was measured following the manufacturer's instructions and absorbance was measured using a plate reader (Tecan Sunrise) at $A_{450}$.

## 2.8. Western blot

Western blot analysis was carried out as previously described (Crampton et al., 2012). Cells were lysed in radioimmunoprecipitation assay (RIPA) buffer (50 μl RIPA per $1 \times 10^6$ cells) consisting of 50 mM Tris-HCL, 150 mM NaCl, 1% Triton X-100, 1 mM EDTA, 1 mM sodium fluoride, 1 mM sodium orthovanadate, 1 μg/ml leupeptin and 1 μg/ml pepstatin for 1 h on ice. Total protein concentration was determined using Pierce BCA Protein Assay Kit (Thermo Fisher). Equal concentrations of protein samples were diluted 1:1 with $5\times$ Laemmli loading buffer (126 mM Tris-HCl, 20% glycerol, 4% SDS, 0.02% bromophenol blue) containing 2.5% β-mercaptoethanol and analysed by SDS-PAGE (Bio-Rad, CA, USA). The membrane was incubated in Tris-buffered saline containing 0.05% Tween (TBS-T) and 5% BSA to block non-specific antibody binding for 1 h at room temperature, before being incubated in primary antibodies against AcH3 (1:1000; rabbit polyclonal IgG; Santa Cruz) and β-actin (1:500; mouse polyclonal; Sigma) diluted in 1% BSA in 10 mM PBS overnight at 4 °C with constant agitation. The membrane was washed, incubated for 1 h with peroxidase conjugate antibody (1:2500; Promega) and staining was detected by enhanced chemiluminescence (GE Healthcare). Protein expression was normalised to Ponceau staining by densitometry using ImageJ.

## 2.9. Statistical analysis

Statistical analysis was performed using GraphPad Prism 8 (©2020 GraphPad Software, CA USA). All data are presented as the mean ± SEM of the number of experimental replicates rather than the number of cells. Statistical differences were analysed using Student's t-test, one-way ANOVA or two-way ANOVA as appropriate, with the post-hoc test as indicated in the figure legends.

## 3. Results

### 3.1. Co-expression analysis implicates specific HDACs in midbrain DA neuron development and function

We first investigated whether any of the HDAC subtypes were significantly co-expressed with markers of human DA SN neurons. This approach is based on the hypothesis that a positive co-expression correlation can reflect a functional association (Homouz and Kudlicki, 2013) (Fig. 1A). To investigate this, we used data from human SN dataset (GSE: 60863) (Ramasamy et al., 2014) and performed a Pearson correlation with Bonferroni post hoc analysis, demonstrating that HDAC3, HDAC5, HDAC6 and HDAC9 display positive correlations with the DA neuronal markers SLC6A3 and NR4A2 (Fig. 1B). To gain further insight into the potential roles of these HDACs in DA neurons, we used RT-qPCR to quantify the expression of their mRNAs during embryonic development of the mouse VM. We discovered that Hdac3 (Fig. 1C), Hdac5 (Fig. 1D), Hdac6 (Fig. 1E) and Hdac9 (Fig. 1F) mRNA levels increased in the developing VM from E10 to reach a peak at E12-E14. Following this peak of expression, the levels of all four of these Hdac mRNAs decreased markedly between E14 and E16, after which expression levels remained approximately stable until birth.

### 3.2. Class-specific HDAC inhibitors

In this study, we evaluated the neurotrophic potential of individual HDIs based on their structure and their abilities to selectively inhibit specific HDAC subtypes in SH-SY5Y cells, which express HDAC3, HDAC5, HDAC6, and HDAC9 (Supplementary Fig. 1). For Class I HDAC inhibition we used RGFP109, a pimelic diphenylamide small molecule which inhibits HDAC1 and HDAC3 with an IC$_{50}$ of 60 nM and 50 nM, respectively (Rai et al., 2010). As a second inhibitor of Class I, we choose RGFP966, which inhibits HDAC3 specifically with an IC$_{50}$ of 0.08 μM and does not have any effects on other HDACs up to a concentration of 15 μM (Thaler and Mercurio, 2014). For inhibition of Class IIa HDACs, we firstly examined LMK235, a highly selective inhibitor of HDAC4 and HDAC5 with an IC$_{50}$ of 11.9 nM and 4.22 nM, respectively (Marek et al., 2013). The second Class IIa-specific HDI examined, TMP269, inhibits all



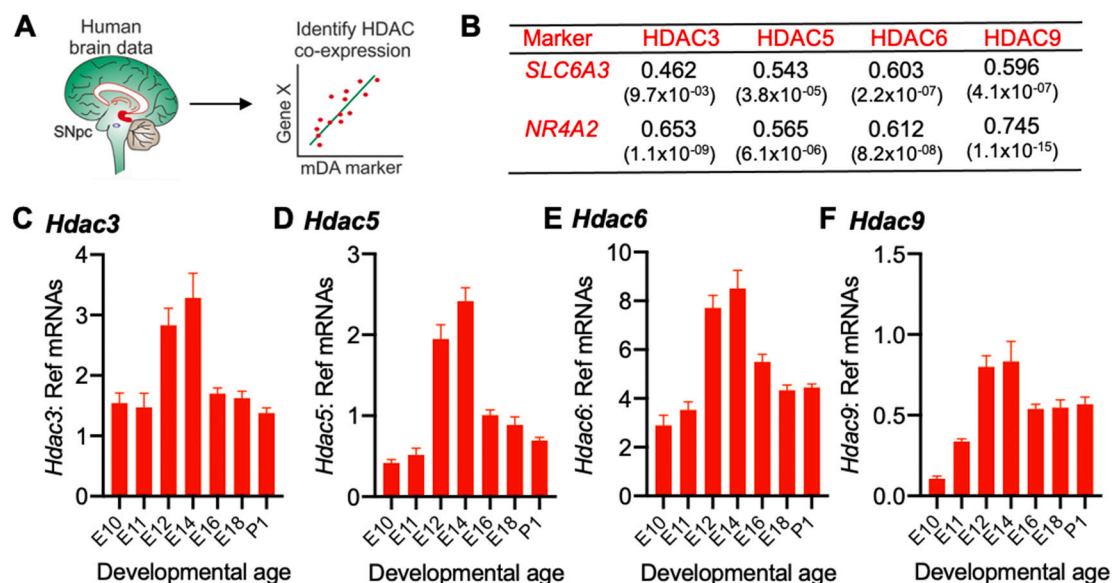| Marker | HDAC3 | HDAC5 | HDAC6 | HDAC9 |
|--------|-------|-------|-------|-------|
| SLC6A3 | 0.462 ($9.7\times10^{-03}$) | 0.543 ($3.8\times10^{-05}$) | 0.603 ($2.2\times10^{-07}$) | 0.596 ($4.1\times10^{-07}$) |
| NR4A2 | 0.653 ($1.1\times10^{-09}$) | 0.565 ($6.1\times10^{-06}$) | 0.612 ($8.2\times10^{-08}$) | 0.745 ($1.1\times10^{-15}$) |

**Fig. 1.** Co-expression analysis implicates specific HDACs in midbrain DA neuron development and function.
(A) Schema showing the experimental approach. Raw data were derived from data set GSE60863 and analysed using the R2 microarray platform. (B) Pearson correlation analyses between each HDAC and SLC6A3 and NR4A2 (markers of DA neurons) in the human SN with the r and Bonferroni-corrected p-values shown in parentheses. (C–F) RT-qPCR of mRNA levels of (C) Hdac3, (D) Hdac5, (E) Hdac6 and (F) Hdac9 in the mouse midbrain from E10 to P1, relative to the levels of the geometric mean of three reference mRNAs; Gapdh, Sdha and Hprt1. Data are presented as the mean ± SEM from 3 to 6 from separate animals at each time point.

subtypes, HDAC 4,5,7 and 9 with an $IC_{50}$ of 126, 80, 36, and 9 nM, respectively (Lobera et al., 2013). To inhibit Class IIb HDACs, we used the HDAC6-specific inhibitor, ACY1215 (Ricolinostat) which has an $IC_{50}$ of 4.7 nM (Santo et al., 2012). For a full summary of the pharmacological HDIs used in this study, see Table 1.

### 3.3. Class I HDAC inhibitors do not affect neurite growth or survival in SH-SY5Y cells

We first examined the effects of class I-specific HDIs on neurite growth and cell viability in SH-SY5Y cells. To do this, SH-SY5Y cells were treated daily with increasing concentrations (0.001–0.1 μM) of RGFP109 (a HDAC1 and HDAC3 inhibitor) or RGFP966 (a HDAC3 selective inhibitor) (Table 1) for 72 h. We first evaluated the potential of each molecule to increase the levels of histone acetylation, using immunocytochemical staining for histone acetylation (acH3-K9.K14) as a readout of HDAC inhibition. We found that RGFP109 resulted in a significant increase in acH3-K9.K14 at a concentration of 0.1 μM, whereas RGFP966 induced a significant increase in acH3-K9.K14 at all tested concentrations (Fig. 2a, d). We next examined the effects of these molecules on neurite growth and cell viability, as readouts of neurotrophic action. Treatment with RGFP109 or RGFP966 for 72 h did not promote neurite growth at any concentration tested (Fig. 2b, e). We also carried out an LDH assay to examine the effects of RGFP109 or RGFP966 on cell survival. Treatment with RGFP109 or RGFP966 for 72 h had no significant effect on cell viability (Fig. 2c,f). Collectively, these data show that, despite an increase in acH3-K9.K14 levels, small molecule inhibitors of HDAC1 and/or HDAC3 do not affect basal neurite outgrowth or cell viability in SH-SY5Y cells.

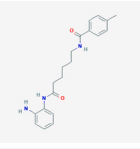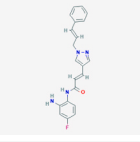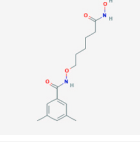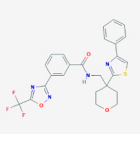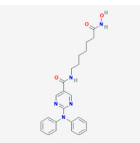### 3.4. Class IIa HDAC inhibitors promote neurite growth in SH-SY5Y cells

We next examined the effects of the class IIa-specific HDIs, LMK235 (a HDAC4/5 inhibitor) and TMP269 (a HDAC9 > HDAC7 > HDAC5 > HDAC4 inhibitor) (Table 1) on neurite growth and cell viability in SH-SY5Y cells. To do this, SH-SY5Y cells were treated daily with increasing concentrations (0.001–0.1 μM) of LMK235 or TMP269 for 72 h. Treatment with LMK235, but not with TMP269, resulted in a significant increase in acH3-K9.K14 (Fig. 3a, d, g). To confirm the effect of LMK235 on acH3-K9.K14 levels, we carried out Western blotting which showed that LMK235 treatment led to a significant increase in acH3-K9.K14 (Supplementary Fig. 2). We next examined the effects of LMK235 and TMP269 on neurite growth. Interestingly, both compounds led to significant increases in neurite growth (Fig. 3b, e, h). LDH assays confirmed that, while there were no significant differences in cells treated with LMK235 compared to control cells, those treated with TMP269 at a concentration of 0.01 μM had significantly lower levels of LDH (Fig. 3c, f). Collectively, these data show that the HDAC4/5 inhibitor, LMK235, and also the pan-class IIa HDAC inhibitor TMP269, increase acH3-K9.K14 levels and promote neurite growth in SH-SY5Y cells.

### 3.5. The HDAC6-specific inhibitor ACY1215 does not affect acetylation levels, neurite outgrowth or cell viability in SH-SY5Y cells

We next examined the effect of HDAC6-specific inhibition using ACY1215, despite the fact that HDAC6 overexpression has previously been demonstrated to have a beneficial effect in *Drosophila* neurodegenerative models (Pandey et al., 2007). To do this, we examined the effects of the HDAC6-specific inhibitor, ACY1215 (Table 1), on neurite growth and cell viability. SH-SY5Y cells were treated daily with increasing concentrations (0.001–0.1 μM) of ACY1215 for 72 h. We found that ACY1215 treatment had no effect on acH3-K9.K14 levels (Fig. 4a, d). This was not surprising given that previous reports described the main function of HDAC6 as a regulator of tubulin acetylation rather than histone acetylation/deacetylation (Hubbert et al.,

**Table 1**

Names and structures of the HDAC inhibitors used in this study.

| Name | IUPAC name | HDAC class specificity | IC50 HDACs subtype (μM) | Chemical structure |
|---|---|---|---|---|
| RGFP109[a] | *N*-[6-(2-aminoanilino)-6-oxohexyl]-4-methylbenzamide | Class I | HDAC1 = 0.060[f] HDAC3 = 0.050[f] | |
| RGFP966[b] | (*E*)-*N*-(2-amino-4-fluorophenyl)-3-[1-[(*E*)-3-phenylprop-2-enyl]pyrazol-4-yl]prop-2-enamide | Class I | HDAC3 = 0.008[g] | |
| LMK235[c] | *N*-[6-(hydroxyamino)-6-oxohexoxy]-3,5-dimethylbenzamide | Class IIa | HDAC4 = 0.012[h] HDAC5 = 0.004[h] | |
| TMP269[d] | *N*-[[4-(4-phenyl-1,3-thiazol-2-yl)oxan-4-yl]methyl]-3-[5-(trifluoromethyl)-1,2,4-oxadiazol-3-yl]benzamide | Class IIa | HDAC9 = 0.023[i] HDAC7 = 0.040[i] HDAC5 = 0.10[i] HDAC4 = 0.13[i] | |
| ACY1215[e] | *N*-[7-(hydroxyamino)-7-oxoheptyl]-2-(*N*-phenylanilino)pyrimidine-5-carboxamide | Class IIb | HDAC6 = 0.005[j] | |

[a] PubChem Database. CID=56654642. https://pubchem.ncbi.nlm.nih.gov/compound/rg2833 (accessed on Apr. 24, 2020).

[b] PubChem Database. CID=56650312. https://pubchem.ncbi.nlm.nih.gov/compound/rgfp966 (accessed on Apr. 24, 2020).

[c] PubChem Database. CID 71520717. https://pubchem.ncbi.nlm.nih.gov/compound/lmk-235 (accessed on Apr. 24, 2020).

[d] PubChem Database. CID 53344908. https://pubchem.ncbi.nlm.nih.gov/compound/tmp269 (accessed on Apr. 24, 2020).

[e] PubChem Database. CID=53340666. https://pubchem.ncbi.nlm.nih.gov/compound/Ricolinostat (accessed on Apr. 24, 2020).

[f] M. Rai, E. Soragni, C.J. Chou, G. Barnes, S. Jones, J.R. Rusche, J.M. Gottesfeld, M. Pandolfo, Two new pimelic diphenylamide HDAC inhibitors induce sustained frataxin upregulation in cells from Friedreich's ataxia patients and in a mouse model, PLoS One 5(1) (2010) e8825.

[g] F. Thaler, C. Mercurio, Towards selective inhibition of histone deacetylase isoforms: what has been achieved, where we are and what will be next, ChemMedChem 9(3) (2014) 523–6.

[h] L. Marek, A. Hamacher, F.K. Hansen, K. Kuna, H. Gohlke, M.U. Kassack, T. Kurz, Histone deacetylase (HDAC) inhibitors with a novel connecting unit linker region reveal a selectivity profile for HDAC4 and HDAC5 with improved activity against chemoresistant cancer cells, Journal of medicinal chemistry 56(2) (2013) 427–36.

[i] M. Lobera, K.P. Madauss, D.T. Pohlhaus, Q.G. Wright, M. Trocha, D.R. Schmidt, E. Baloglu, R.P. Trump, M.S. Head, G.A. Hofmann, M. Murray-Thompson, B. Schwartz, S. Chakravorty, Z. Wu, P.K. Mander, L. Kruidenier, R. A. Reid, W. Burkhart, B.J. Turunen, J.X. Rong, C. Wagner, M.B. Moyer, C. Wells, X. Hong, J.T. Moore, J.D. Williams, D. Soler, S. Ghosh, M.A. Nolan, Selective class IIa histone deacetylase inhibition *via* a nonchelating zinc-binding group, Nat Chem Biol 9(5) (2013) 319–25.

[j] L. Santo, T. Hideshima, A.L. Kung, J.C. Tseng, D. Tamang, M. Yang, M. Jarpe, J.H. van Duzer, R. Mazitschek, W.C. Ogier, D. Cirstea, S. Rodig, H. Eda, T. Scullen, M. Canavese, J. Bradner, K.C. Anderson, S.S. Jones, N. Raje, Preclinical activity, pharmacodynamic, and pharmacokinetic properties of a selective

HDAC6 inhibitor, ACY-1215, in combination with bortezomib in multiple myeloma, Blood 119(11) (2012) 2579–89.

All information in this table is from the National Center for Biotechnology Information (NCBI) (https://pubchem.ncbi.nlm.nih.gov).

2002). Despite this, we assessed the effect of ACY1215 on neurite growth. We found that ACY1215 did not increase neurite growth at any of the tested concentrations (Fig. 4b, e). LDH assay showed that ACY1215 treatment had no significant effect on cell viability (Fig. 4e). Collectively, these data show that the small molecule HDAC6 inhibitor, ACY1215, had no effect on acH3-K9.K14 levels, neurite outgrowth and viability in SHSY5Y cells.

### 3.6. The effects of LMK235 on neurite growth require BMP-Smad pathway activation in SH-SY5Y cells

We next sought to explore the potential mechanisms underlying the beneficial effects of LMK235. We hypothesised that these effects may be mediated through activation of the BMP-Smad signalling pathway, as we have previously shown that this pathway is required for promoting neurite growth following HDAC5 inhibition (Mazzocchi et al., 2019). Firstly, SH-SY5Y cells were transfected with a Smad-GFP reporter

construct to quantify Smad-dependent transcription and then cells were treated with 0.1 μM of LMK235 for 24 h. We found that LMK235 treatment resulted in a significant increase in GFP fluorescence intensity compared to the control (Fig. 5a, b). To confirm this, we treated SH-SY5Y cells with 0.1 μM of LMK235 for 24 h and then immunocytochemically stained for pSmad1/5 as a readout of activation of the BMP-Smad pathway. The 24 h time point was used to minimise the potential for negative feedback inhibition of the pathway and because we found that 72 h treatment with dorsomorphin adversely affects cell viability (data not shown).We found that LMK235 treatment resulted in a significant increase in pSmad1/5, which was prevented by co-treatment with dorsomorphin, a small molecule known to block BMP pathway activation (Yu et al., 2008) (Fig. 5c). Similar findings were also seen in cultures transfected with siRNAs targeting HDAC5 (Supplementary Fig. 3). To confirm these findings in DA neurons, we next treated primary cultures of E14 rat VM for 24 h with 0.02 μM of LMK235, a concentration which has previously been used in primary neuronal cultures (Trazzi et al., 2016), and immunocytochemically stained them for TH and pSmad1/5. Densitometry analysis revealed that LMK235 treatment led to a significant increase in pSmad1/5 levels in TH^{+} neurons, which was prevented by dorsomorphin (Fig. 5d). To determine whether the effect of LMK235 on neurite growth was mediated through the BMP-
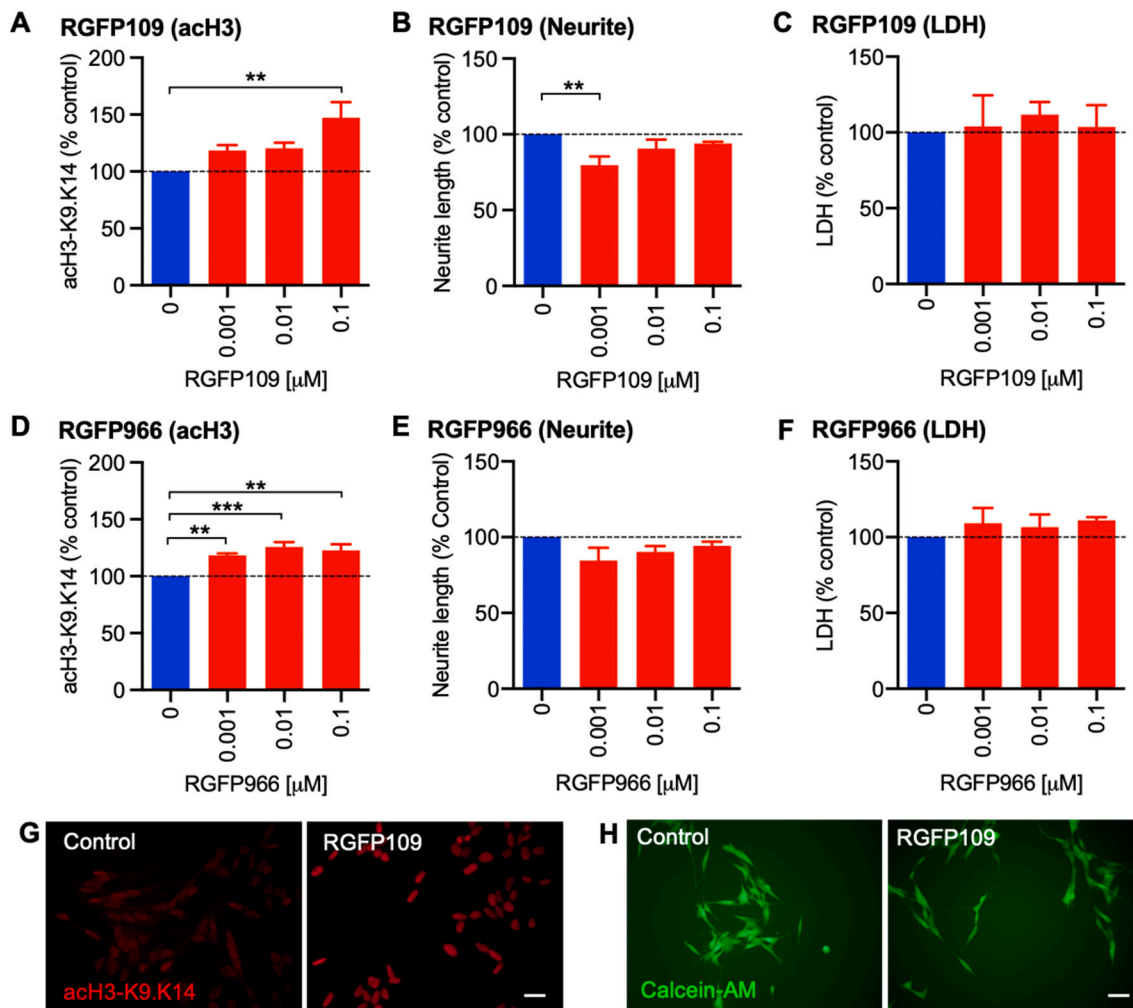


**Fig. 2.** Class I-specific HDAC inhibitors promote histone acetylation but do not affect neurite growth in SH-SY5Y cells. Graphs of (A, D) acetylated histone H3 levels (acH3-K9.K14), (B, E) neurite length and (C, F) LDH activity as a readout of cell viability of SH-SY5Y cells cultured either without HDI's or treated daily with the indicated concentrations of the HDIs RGFP109 or RGFP966 for 72 h. All data are presented as the mean ± SEM as a percentage of the control of $n = 3$ experiments. ** $p < 0.01$; *** $p < 0.001$ *vs.* control (0 μM group). One-way ANOVA with *post hoc* Fishers LSD test. (G, H) Representative photomicrographs of control SH-SY5Y cells and SH-SY5Y cells treated with increasing concentration of RGFP109 (0.001–0.1 μM) showing (G) immunocytochemistry for acH3-K9.K14 and (H) SH-SY5Y cells stained with the vital fluorescent dye Calcein-AM to visualise neurites. Scale bar = 25 μm.
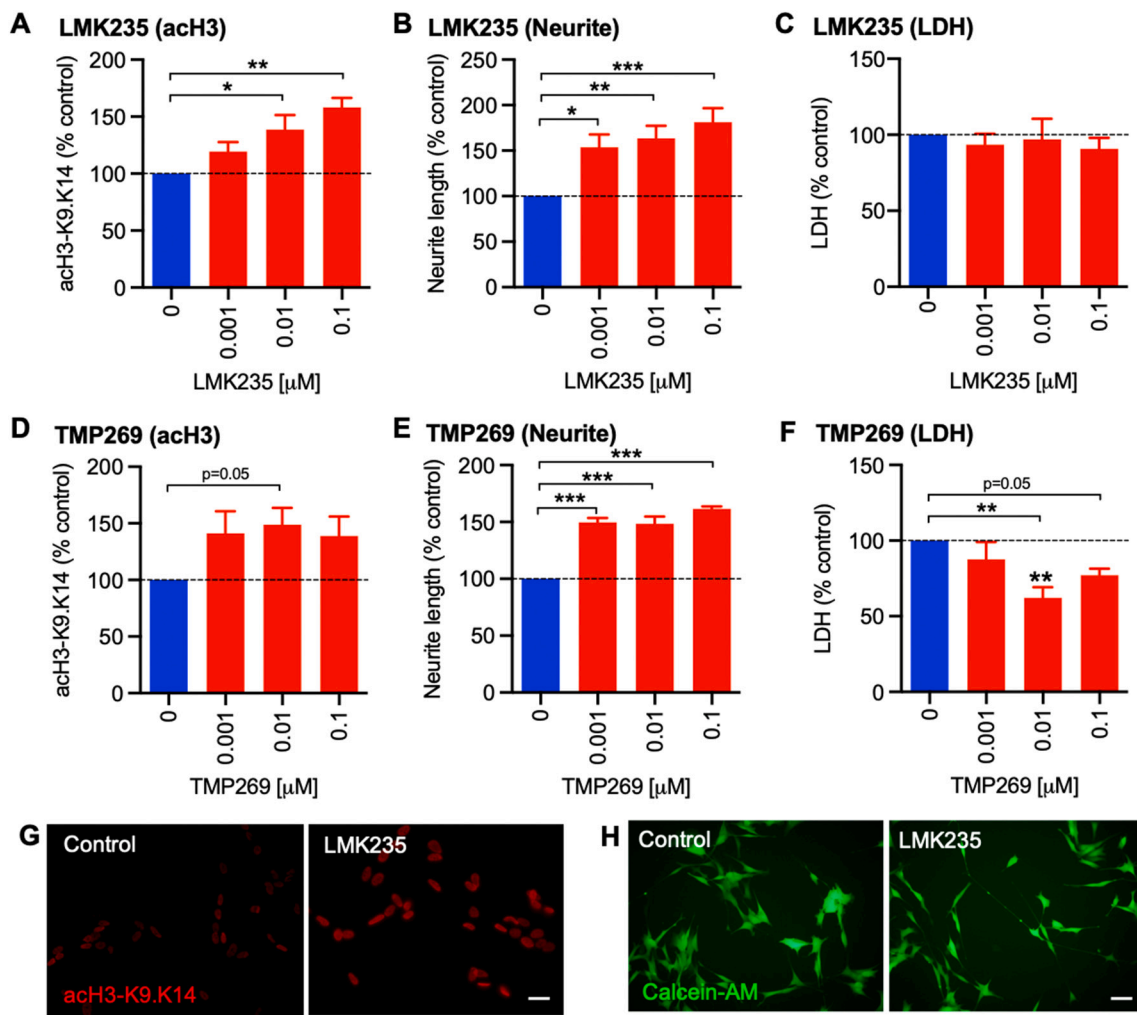
**Fig. 3.** Class IIa HDAC inhibitors promote histone acetylation and neurite growth in SH-SY5Y cells. Graphs of (A, D) acetylated histone H3 levels (acH3-K9.K14), (B, E) neurite length and (C, F) LDH activity as a readout of cell viability of SH-SY5Y cells cultured either without HDI's or treated daily with the indicated concentrations of the HDIs LMK235 or TMP269 for 72 h. All data are presented as the mean ± SEM as a percentage of the control of $n = 3$ experiments. ** $p < 0.01$; *** $p < 0.001$ *vs.* control (0 μM group). One-way ANOVA with *post hoc* Fishers LSD test. (G, H) Representative photomicrographs of control SH-SY5Y cells and SH-SY5Y cells treated with 0.1 μM LMK235 showing (G) immunocytochemistry for acH3-K9.K14 and (H) SH-SY5Y cells stained with the vital fluorescent dye Calcein-AM to visualise neurites. Scale bar = 25 μm.

Smad pathway, we examined neurite growth in SH-SY5Y cells and E14 VM cultures treated with LMK235 with or without dorsomorphin and found that dorsomorphin inhibited the neurite growth-promoting effects of LMK235 in SH-SY5Y cells (Fig. 5e) and in DA neurons (Fig. 5f). Collectively, these data show that LMK235 activates the BMP-Smad pathway and is required for the beneficial effects of LMK235 on neurite growth.

### 3.7. LMK235 protects against MPP$^+$-induced neurotoxicity in SH-SY5Y cells and E14 VM primary cultures

Since LMK235 was the only compound to increase acH3-K9.K14 levels and to promote neurite growth, but had no adverse effects on cell viability, we next examined whether LMK235 could protect against the detrimental effects of MPP$^+$ on neurite growth. Firstly, we treated SH-SY5Y cells with 1 mM MPP$^+$ and cultured them with or without 0.1 μM LMK235 for 72 h. We found that LMK235 treatment partially rescued MPP$^+$-induced reductions in neurite length (Fig. 6a). We sought to confirm these findings in DA neurons. To do this, we treated primary cultures of E14 rat VM with 1 mM MPP$^+$ with or without 0.02 μM of LMK235 for 24 h. MPP$^+$ and LMK235 were added simultaneously. We found that, while MPP$^+$-induced degeneration resulted in significant

reductions in neurite length (Fig. 6b, d) and in the numbers of DA neurons per field (Fig. 6c, d), LMK235 protected against MPP$^+$-induced degeneration (Fig. 6b–d). Collectively these data show that a small molecule inhibitor of HDAC4/5 can protect against MPP$^+$-induced degeneration in SH-SY5Y cells and DA neurons.

### 3.8. LMK235 protects against AAV2/6-α-Synuclein-induced neurodegeneration in SH-SY5Y cells and E14 VM primary cultures

While MPP$^+$ treatment models the oxidative stress-induced changes in PD at the cellular level, PD in patients is characterised by the accumulation of α-synuclein. Therefore, we next examined whether LMK235 could protect against the detrimental effects of WT or A53T-α-synuclein. To do this, SH-SY5Y cells were transfected with a Control-GFP plasmid, or a plasmid expressing GFP-tagged A53T α-synuclein (αSynA53T-GFP) or WT α-synuclein (αSyn-GFP) and then treated with 0.1 μM of LMK235 for 72 h. Cultures were fixed and stained for acH3-K9.K14 to quantify histone acetylation, while images of GFP-positive cells were used for analysing neurite growth. Neurite length analysis showed that LMK235 treatment protected against the detrimental effects of αSynA53T-GFP on neurite growth (Fig. 7a). Moreover, LMK235-treated αSynA53T-GFP-expressing cells had higher levels of acH3-K9.K14 (Fig. 7b). In similar
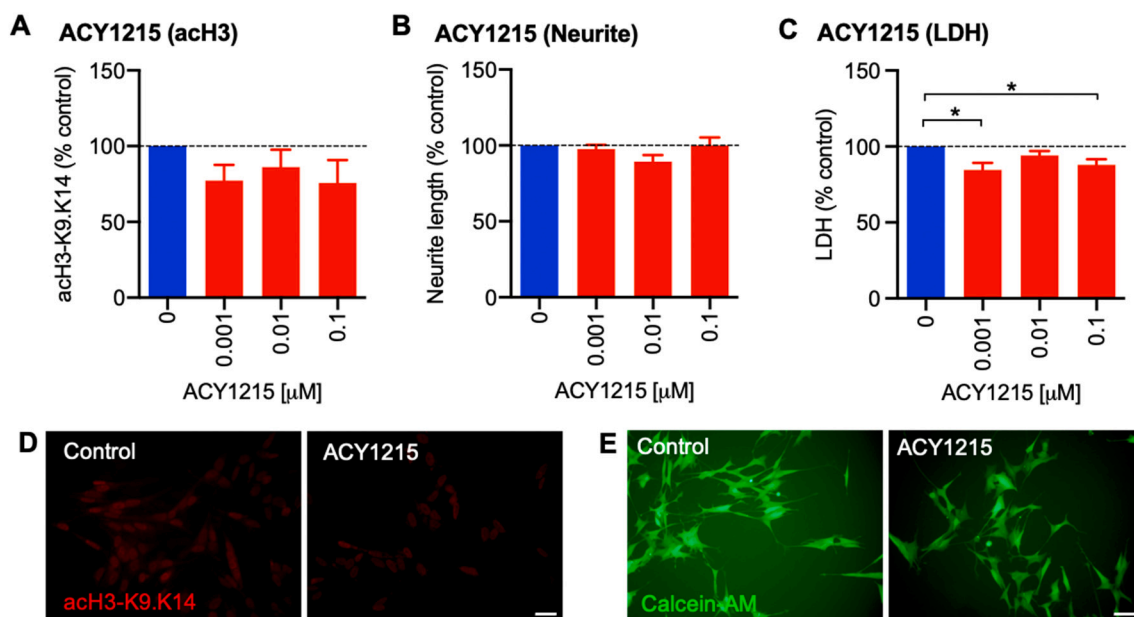
**Fig. 4.** The Class IIb HDAC6 inhibitor ACY1215 does not promote histone acetylation or neurite growth in SH-SY5Y cells. Graphs of (A) acetylated histone H3 levels (acH3-K9.K14), (B) neurite length and (C) LDH activity as a readout of cell viability of SH-SY5Y cells cultured either without HDIs or treated daily with the indicated concentrations of the HDI ACY1215 for 72 h. All data are presented as the mean ± SEM as a percentage of the control of $n = 3$ experiments. * $p < 0.05$ *vs.* control (0 μM group). One-way ANOVA with *post hoc* Fishers LSD test. (G, H) Representative photomicrographs of control SH-SY5Y cells and SH-SY5Y cells treated with 0.1 μM ACY1215 showing (D) immunocytochemistry for acH3-K9.K14 and (E) SH-SY5Y cells stained with the vital fluorescent dye Calcein-AM to visualise neurites. Scale bar =25 μm.
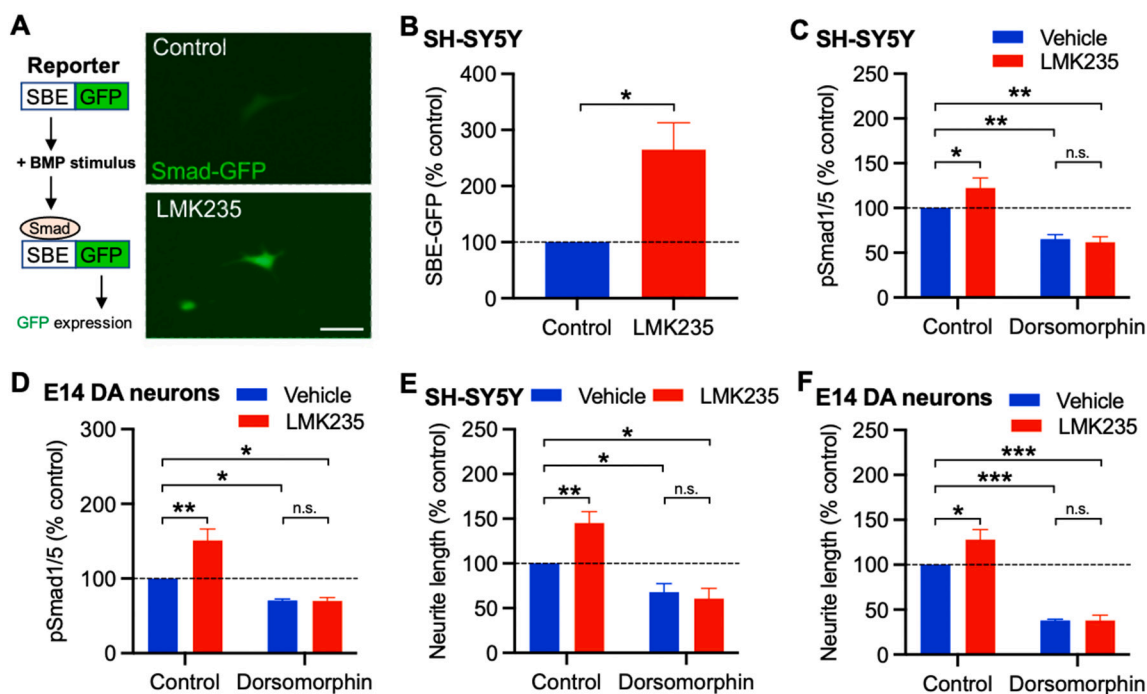


**Fig. 5.** LMK235 induces Smad activation, which is required for its effect on neurite growth in SH-SY5Y cells. (A) Schema and representative photomicrographs and (B) graph of GFP expression (as a measurement of Smad-dependent transcription) in SH-SY5Y cells transfected with a Smad-GFP reporter construct and treated with 0.1 μM LMK235 for 24 h. (C) Graph showing densitometry of phospho-(p)Smad1/5 staining in SH-SY5Ycells at 24 h when treated daily with either vehicle or 0.1 μM LMK235, with or without pre-treatment with 1 μg/ml dorsomorphin. (D) Graph showing densitometry of phospho-(p)Smad1/5 staining in E14 rat VM cultures at 24 h when treated with either vehicle or 0.02 μM LMK235, with or without pre-treatment with 1 μg/ml dorsomorphin. (E) Graph showing neurite length analysis in SH-SY5Y cells treated with either vehicle or 0.1 μM LMK235 for 24 h, with or without pre-treatment with 1 μg/ml dorsomorphin. (F) Graph showing neurite length of TH-positive DA neurons in primary cultures of E14 rat VM cultured either with or without 0.02 μM of LMK235 for 24 h, with or without pre-treatment with 1 μg/ml dorsomorphin. All data are presented as the mean ± SEM as a percentage of the control of $n = 3$ experiments. * $p < 0.05$; ** $p < 0.01$; *** $p < 0.001$ *vs.* control or as indicated; n.s. = not significant. One-way ANOVA with *post hoc* Fishers LSD test. Scale bar = 100 μm.
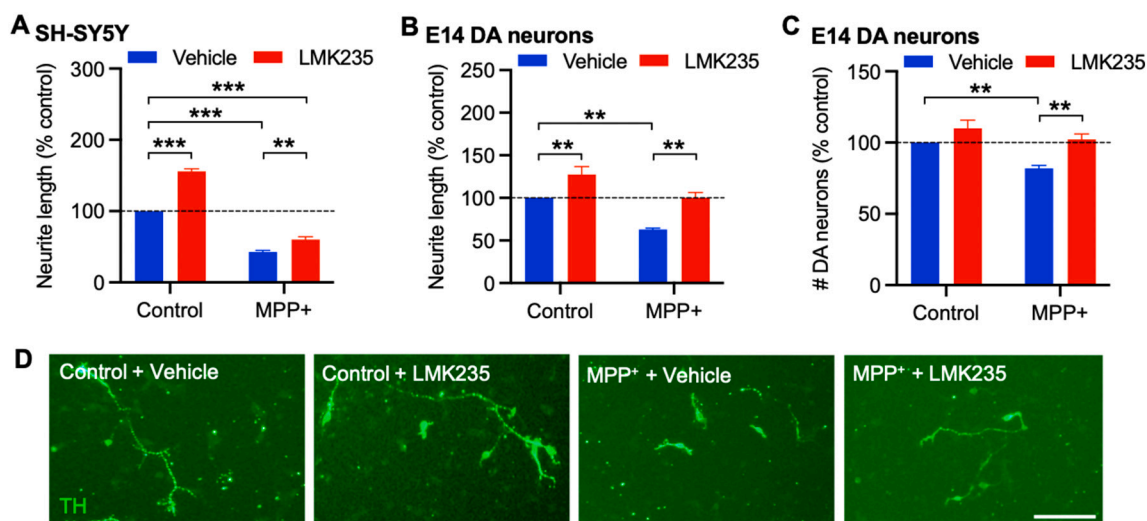
**Fig. 6.** LMK235 protects against MPP$^+$-induced neurotoxicity in SH-SY5Y cells and E14 VM primary cultures. (A) Graph showing neurite length of SH-SY5Y cells at 72 h when cultured with or without 1 mM MPP$^+$ and supplemented daily with either vehicle or 0.1 μM LMK235. Graphs of (B) neurite length and (C) neuron number, and (D) representative photomicrographs of tyrosine hydroxylase (TH)-positive DA neurons in primary cultures of E14 rat VM at 72 h cultured either with or without 1 mM MPP$^+$ and supplemented with either vehicle with or 0.02 μM of LMK235. MPP$^+$ and LMK235 were added simultaneously. All data are presented as the mean ± SEM as a percentage of the control of $n = 3$ experiments. ** $p < 0.01$; *** $p < 0.001$ vs. control or as indicated; One-way ANOVA with post hoc Fishers LSD test. Scale bar = 100 μm.

experiments with WT α-synuclein, LMK235 treatment also protected against the detrimental effects of αSyn-GFP on neurite growth (Fig. 7c). There were no significant differences in acH3-K9.K14 levels, but a trend towards an increased level was observed (Fig. 7d). Finally, we sought to determine if LMK235 exerted beneficial effects on cultured DA neurons with an established α-synuclein burden. To do this, primary cultures of E14 rat VM were transduced with AAV-GFP or AAV-αSyn vectors. This led to strong expression of human WT α-synuclein at 5 days post-transduction in cultures transduced with AAV-αSyn (Fig. 7e). At 5 days post-transduction, cultures were cultured for a further 5 DIV with or without daily treatment of 0.02 μM of LMK235. An analysis of neurite growth revealed that AAV-αSyn resulted in a significant reduction in DA neurite length compared to the AAV-GFP control group, which was not seen in AAV-αSyn cultures treated with LMK235 (Fig. 7f). Collectively, these data show that LMK235 protects against α-synuclein-induced degeneration of DA neurons in vitro.

## 4. Discussion

Despite the many studies that have focused on the connection between PD and the processes of histone acetylation/deacetylation, the exact role of individual HDACs in PD pathology is still largely unknown. In this context, pan-HDIs have been extensively studied as potential therapeutic agents for PD (Dietz and Casaccia, 2010; Hegarty et al., 2016b). However, there have been several contrasting results, suggesting that some HDACs may have potential neuroprotective roles (Kidd and Schneider, 2011; Mazzocchi et al., 2019; Paiva et al., 2017), while others may exacerbate the neurodegenerative state (Harrison et al., 2019; Wang et al., 2009). Furthermore, given that distinct HDACs are expressed in different cells and tissues, a lack of specificity in targeting HDAC subtypes may lead to side effects. In this study, we performed co-expression analysis to verify whether any HDAC subtypes were significantly correlated with DA markers of human SN, to explore possible functional correlations. We found that the expression of HDAC3, 5, 6 and 9 was positively correlated with that of the DA markers. We then confirmed that all of these HDAC subtypes were expressed at the mRNA level in developing embryonic mouse DA neurons, with these expression patterns suggesting potential roles in midbrain DA (mDA) axonal growth. Next, we examined the effect of class-specific HDAC inhibition

using a range of pharmacological inhibitors to separately assess the effects of the class-specific HDIs, RGFP966, RGFP109, LMK235, TMP269 and ACY1215, on cell survival and neurite growth. We found that only class IIa inhibition resulted in increases in neurite growth and in histone acetylation. In addition, LMK235, which is an inhibitor of HDAC4 and HDAC5, protected both SH-SY5Y cells and cultured DA neurons from the toxic effects of MPP$^+$. The reductions in neurite growth induced by overexpression of WT and A53T α-synuclein in SH-SY5Y cells, and of WT α-synuclein in cultured DA neurons, were also prevented by LMK235. Finally, we found that the beneficial effects of LMK235 were mediated by activation of the BMP-Smad signalling pathway.

Firstly, we examined the effects of class-I HDIs RGFP109 and RGFP966 on the levels of histone acetylation and neurite outgrowth. We found a dose-dependent increase in acetylation of histone 3 levels after treatment with RGFP109, while RGFP966 induced increases at all of the concentrations tested. These increases in histone acetylation induced by RGFP109 or RGFP966 were not coupled with increases in neurite length. In agreement, a study on dorsal root ganglion (DRG) neurons found that HDAC3 genetic or pharmacological inhibition increased levels of acetylation of histone 3 after spinal cord injury in vivo (Hervera et al., 2019). However, in contrast to our findings, that study also showed that inhibition of HDAC3 induced increases in axon length. A ChIP seq of histone 3 lysine 6 (H3K9) demonstrated that HDAC3 is involved in the regulation of regenerative pathways (Hervera et al., 2019). On the other hand, in support of our finding, another study demonstrated that class-I-specific inhibitors PCI-34051 and MS-275 had no effect on neurite growth or branching after 24 h treatment of SH-SY5Y cells (Collins et al., 2015).

Secondly, we examined the ability of the class-IIa HDIs, LMK235 and TMP269 to increase histone acetylation and promote neurite growth. We found that both compounds induced increases in neurite length that were coupled with increases in H3 acetylation. In agreement with this, a previous study found that class IIa inhibition using the class IIa HDI, MC1568, promoted axon growth in both mDA and sympathetic neurons in vitro (Collins et al., 2015). In further support of these findings, our previous study used short interfering RNA (siRNA) to show that inhibition of HDAC5 or HDAC9, but not of HDAC4 or HDAC7, induced neurite outgrowth in both SH-SY5Y cells and cultured DA neurons (Mazzocchi et al., 2019). In the same study it was also confirmed that
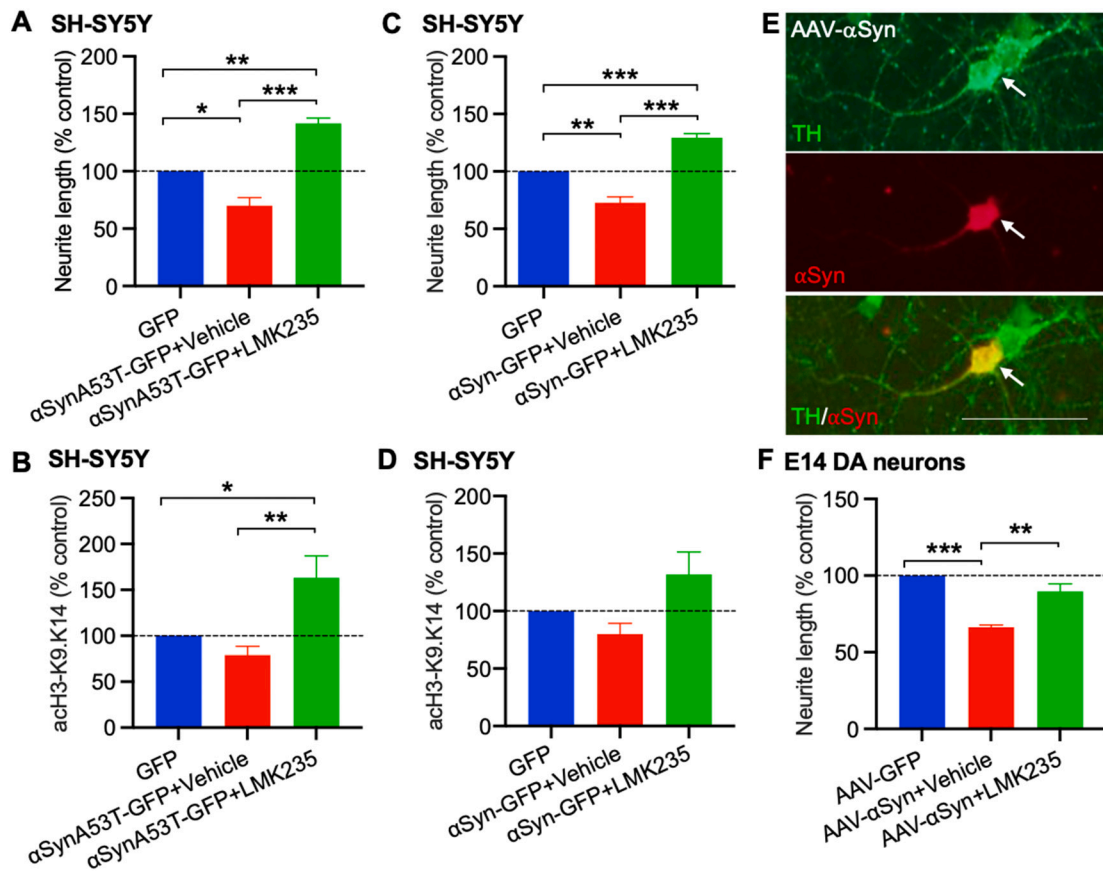
**Fig. 7.** LMK235 protects against AAV2/6-α-Synuclein-induced neurodegeneration in SH-SY5Y cells and E14 VM primary cultures. (A-–D) Graphs showing (A, C) neurite length and (B, D) the relative levels of acetylated histone 3 (acH3.K9.K14) of SH-SY5Y cells at 72h when treated daily with 0.1 μM LMK235 or vehicle and transfected with a plasmid overexpressing (A, B) α-synuclein (αSynA53T-GFP) or (C, D) wild-type α-synuclein (αSyn-GFP). Cells were transfected with a GFP-expressing plasmid as a control. (E) Representative photomicrographs showing human α-synuclein staining (red) in TH-positive DA neurons (green) in primary cultures of E14 rat 5 days post transduction with an AAV vector carrying the WT human α-synuclein gene (AAV-αSyn). Control cultures were transduced with AAV-GFP. (F) Graph showing neurite length of DA neurons in primary cultures of E14 rat VM at 10 days post-transduction with AAV-GFP or AAV-αSyn. In a delayed treatment paradigm, where indicated, cultures were treated with either vehicle or 0.02 μM LMK235 daily from days 5–10. All data are presented as the mean ± SEM as a percentage of the control of $n = 3$ experiments. * $p < 0.05$; ** $p < 0.01$; *** $p < 0.001$ vs. control or as indicated; One-way ANOVA with post-hoc Fisher's LSD test. Scale bar = 50 μm.

class IIa-specific inhibition using MC1568 led to an increase in histone 3 acetylation levels (Mazzocchi et al., 2019). Moreover, a study by Sugo et al. demonstrated that shRNA-mediated inhibition of HDAC9 led to a significant increase in dendritic length and complexity of branching in cultured cortical neurons (Sugo et al., 2010). In support of our findings, Cho et al. reported that HDAC5 nuclear export is essential for regeneration of DRG neurons after injury, both in vitro and in vivo (Cho et al., 2013). Interestingly, HDAC5 nuclear export after injury resulted in an increase in acetylation of histone 3 (Cho et al., 2013). This suggests that the beneficial effects of HDAC5 inhibition may not be cell type-specific and could be triggered using specific pharmacological inhibition.

We next examined the ability of the HDAC6-specific inhibitor ACY1215 to increase the level of histone 3 acetylation and neurite growth. We found that ACY1215 had no significant effect on the levels of histone acetylation or on neurite growth. In contrast with our findings, Tapia et al. found that inhibition of HDAC6 using either short hairpin RNA (shRNA) or Tubacin, a HDAC6-specific pharmacological inhibitor, suppressed axon formation and delayed elongation in cultured murine hippocampal neurons (Tapia et al., 2010). However, these effects of HDAC6 may be cell type-specific, as another study used both pharmacological and genetic-mediated inhibition of HDAC6 and reported an increase in neurite outgrowth in cultured cortical neurons (Rivieccio et al., 2009). In this study, it was also reported that the increases in neurite length were coupled with increases in acetylation of α-tubulin,

but not of histone substrates (Rivieccio et al., 2009). This was confirmed by Guo et al. who demonstrated that HDAC6 inhibition using ACY1215 mainly increased α-tubulin acetylation levels which ameliorate axonal transport defect in iPSCs derived from amyotrophic lateral sclerosis patients (Guo et al., 2017). These data collectively suggest that the main target of HDAC6 is α-tubulin homeostasis to affect axonal transport but not axon outgrowth.

Having shown the beneficial effects of LMK235 on neurite growth, we next examined the potential mechanisms that may underlie the neurite growth-promoting effects of LMK235. We found that the beneficial effects of LMK235 on neurite growth were mediated by activation of the BMP-Smad pathway. In accordance with this, previous reports have shown that the pan-Class IIa HDI, MC1568, increased p-Smad1/5/8 levels in a time-dependent manner and led to the activation of the canonical BMP-Smad pathway (Collins et al., 2015). In additional support, our previous study showed that MC1568 administration induced an increase in *SMAD1* and *BMP2* transcript expression in SH-SY5Y cells. In addition, we found that both pharmacological and genetic inhibition of HDAC5 increased neurite growth via activation of the BMP-Smad pathway (Mazzocchi et al., 2019). Furthermore, Taniguchi et al. performed a study on HDAC5 binding sites using ChIP-seq, and showed an association of HDAC5 with the BMP2 promoter region, confirming that HDAC5 could control the expression of BMP2, a BMP-Smad pathway activator (Taniguchi et al., 2017).

We next tested the neuroprotective effects of LMK235, a specific HDAC4/5 inhibitor, in *in vitro* models of PD. We found that LMK235 protected axons from MPP$^+$-induced degeneration of both SH-SY5Y and cultured DA neurons. In support of this, a previous study reported that the pan-class IIa inhibitor, MC1568, protected against MPP$^+$-induced reductions in axonal length and branching in cultured DA and sympathetic neurons (Collins et al., 2015). Previous studies have also reported that the pan-HDIs, sodium butyrate (NaB), valproic acid (VPA) and SAHA, protected against MPP$^+$-induced toxicity in an *in vitro* model of PD (Kidd and Schneider, 2010). Importantly, we also found that LMK235 protected axons from neurodegeneration caused by overexpression of WT or A53T α-synuclein. In accordance with this, a study by Kontopoulos et al. (2006) demonstrated that α-synuclein localised in the nucleus directly inhibits acetylation of histone 3, by physically interacting with histones both *in vitro* and *in vivo*. Furthermore, Paiva et al. (2017) found that NaB, a pan-HDI, reversed the reduction of histone acetylation levels caused by WT α-synuclein overexpression in LUHMES cells. In support of this, we previously demonstrated that siRNA-mediated inhibition of Class IIa HADCs, HDAC5 and HDAC9 protected against α-synuclein-induced reductions in neurite growth (Mazzocchi et al., 2019). Collectively, these data suggest that the neuroprotective effects exerted by pan-HDIs may be mediated by HDAC4/5 inhibition.

Interestingly, a link between Smad activation and class IIa HDACs has previously been reported (Jensen et al., 2009). That study found that treatment of C2C12 cells with BMP2 induces class IIa HDAC nuclear export, with a significant effect on HDAC7. Shuttling of HDAC7 from the nucleus to the cytoplasm, mediated by activation of PKD and CaMK, which induce HDAC7 phosphorylation and consequent nuclear export, induced a negative regulation of the Runx2 transcription factor, suggesting that HDACs and Smad interaction can influence several cellular process (Jensen et al., 2009). Collectively, these data, together with our studies, shows the potential of HDIs as therapeutics for PD and highlights the need for further research on class-specific HDI inhibition. In particular, these findings show that Class IIa inhibitors induce neurotrophic effects on DA neurons which may be applicable to neuroprotective and neurorestorative strategies to treat PD.

In conclusion, we have demonstrated that pharmacological inhibition of Class IIa HDACs, using LMK235, induces neurite outgrowth and protects axons from neurodegeneration through activation of the BMP-Smad signalling pathway, in cellular models of PD. These data confirm HDAC5 as a potential therapeutic target for PD, with a particular focus on early axonal degeneration.

Supplementary data to this article can be found online at https://doi.org/10.1016/j.mcn.2021.103642.

## Funding

## CRediT authorship contribution statement

Martina Mazzocchi, Susan Goulding: cell culture experiments. Martina Mazzocchi: Western blot experiment. Sean Wyatt: RT-qPCR experiments. Martina Mazzocchi, Louise Collins, Aideen Sullivan and Gerard O'Keeffe: analysed data, prepared figures and wrote manuscript. All authors edited final manuscript. Louise Collins, Aideen Sullivan and Gerard O'Keeffe: designed the study and supervised the work.

## Declaration of competing interest

The authors declare that the research was conducted in the absence of any commercial or financial relationships that could be construed as a potential conflict of interest.

## References

Beach, T.G., Adler, C.H., Sue, L.I., Peirce, J.B., Bachalakuri, J., Dalsing-Hernandez, J.E., Lue, L.F., Caviness, J.N., Connor, D.J., Sabbagh, M.N., Walker, D.G., 2008. Reduced striatal tyrosine hydroxylase in incidental Lewy body disease. Acta Neuropathol. 115, 445–451.

Cheung, Y.T., Lau, W.K., Yu, M.S., Lai, C.S., Yeung, S.C., So, K.F., Chang, R.C., 2009. Effects of all-trans-retinoic acid on human SH-SY5Y neuroblastoma as in vitro model in neurotoxicity research. Neurotoxicology 30 (1), 27–35. https://doi.org/10.1016/j.neuro.2008.11.001.

Cho, Y., Sloutsky, R., Naegle, K.M., Cavalli, V., 2013. Injury-induced HDAC5 nuclear export is essential for axon regeneration. Cell 155, 894–908.

Choi, H.K., Choi, Y., Kang, H., Lim, E.J., Park, S.Y., Lee, H.S., Park, J.M., Moon, J., Kim, Y.J., Choi, I., Joe, E.H., Choi, K.C., Yoon, H.G., 2015. PINK1 positively regulates HDAC3 to suppress dopaminergic neuronal cell death. Hum. Mol. Genet. 24, 1127–1141.

Choong, C.J., Sasaki, T., Hayakawa, H., Yasuda, T., Baba, K., Hirata, Y., Uesato, S., Mochizuki, H., 2016. A novel histone deacetylase 1 and 2 isoform-specific inhibitor alleviates experimental Parkinson's disease. Neurobiol. Aging 37, 103–116.

Chu, Y., Morfini, G.A., Langhamer, L.B., He, Y., Brady, S.T., Kordower, J.H., 2012. Alterations in axonal transport motor proteins in sporadic and experimental Parkinson's disease. Brain 135, 2058–2073.

Chun, H.S., Gibson, G.E., DeGiorgio, L.A., Zhang, H., Kidd, V.J., Son, J.H., 2001. Dopaminergic cell death induced by MPP(+), oxidant and specific neurotoxicants shares the common molecular mechanism. J. Neurochem. 76, 1010–1021.

Collins, L.M., Adriaanse, L.J., Theratile, S.D., Hegarty, S.V., Sullivan, A.M., O'Keeffe, G.W., 2015. Class-IIa histone deacetylase inhibition promotes the growth of neural processes and protects them against neurotoxic insult. Mol. Neurobiol. 51, 1432–1442.

Crampton, S.J., Collins, L.M., Toulouse, A., Nolan, Y.M., O'Keeffe, G.W., 2012. Exposure of foetal neural progenitor cells to IL-1beta impairs their proliferation and alters their differentiation - a role for maternal inflammation? J. Neurochem. 120, 964–973.

de Ruijter, A.J., van Gennip, A.H., Caron, H.N., Kemp, S., van Kuilenburg, A.B., 2003. Histone deacetylases (HDACs): characterization of the classical HDAC family. Biochem. J. 370, 737–749.

Dietz, K.C., Casaccia, P., 2010. HDAC inhibitors and neurodegeneration: at the edge between protection and damage. Pharmacol. Res. 62, 11–17.

Furlong, R.A., Narain, Y., Rankin, J., Wyttenbach, A., Rubinsztein, D.C., 2000. Alpha-synuclein overexpression promotes aggregation of mutant huntingtin. Biochem. J. 346 (Pt 3), 577–581. https://doi.org/10.1042/bj3460577.

Guo, W., Naujock, M., Fumagalli, L., Vandoorne, T., Baatsen, P., Boon, R., Ordovas, L., Patel, A., Welters, M., Vanwelden, T., Geens, N., Tricot, T., Benoy, V., Steyaert, J., Lefebvre-Omar, C., Boesmans, W., Jarpe, M., Sterneckert, J., Wegner, F., Petri, S., Bohl, D., Vanden Berghe, P., Robberecht, W., Van Damme, P., Verfaillie, C., Van Den Bosch, L., 2017. HDAC6 inhibition reverses axonal transport defects in motor neurons derived from FUS-ALS patients. Nat. Commun. 8, 861.

Harrison, I.F., Powell, N.M., Dexter, D.T., 2019. The histone deacetylase inhibitor nicotinamide exacerbates neurodegeneration in the lactacystin rat model of Parkinson's disease. J. Neurochem. 148, 136–156.

Hegarty, S.V., O'Leary, E., Solger, F., Stanicka, J., Sullivan, A.M., O'Keeffe, G.W., 2016a. A small molecule activator of p300/CBP histone acetyltransferase promotes survival and neurite growth in a cellular model of Parkinson's disease. Neurotox. Res. 30, 510–520.

Hegarty, S.V., Sullivan, A.M., O'Keeffe, G.W., 2016b. The Epigenome as a therapeutic target for Parkinson's disease. Neural Regen. Res. 11, 1735–1738.

Hegarty, S.V., Sullivan, A.M., O'Keeffe, G.W., 2016c. Protocol for evaluation of neurotrophic strategies in Parkinson's disease-related dopaminergic and sympathetic neurons in vitro. J. Biol. Methods 3, e50.

Hegarty, S.V., Wyatt, S.L., Howard, L., Stappers, E., Huylebroeck, D., Sullivan, A.M., O'Keeffe, G.W., 2017. Zeb2 is a negative regulator of midbrain dopaminergic axon growth and target innervation. Sci. Rep. 7, 8568.

Hervera, A., Zhou, L., Palmisano, I., McLachlan, E., Kong, G., Hutson, T.H., Danzi, M.C., Lemmon, V.P., Bixby, J.L., Matamoros-Angles, A., Forsberg, K., De Virgiliis, F., Matheos, D.P., Kwapis, J., Wood, M.A., Puttagunta, R., Del Rio, J.A., Di Giovanni, S., 2019. PP4-dependent HDAC3 dephosphorylation discriminates between axonal regeneration and regenerative failure. EMBO J. 38, e101032.

Homouz, D., Kudlicki, A.S., 2013. The 3D organization of the yeast genome correlates with co-expression and reflects functional relations between genes. PLoS One 8, e54699.

Hourani, M., Berretta, R., Mendes, A., Moscato, P., 2008. Genetic signatures for a rodent model of Parkinson's disease using combinatorial optimization methods. Methods Mol. Biol. 453, 379–392.

Hubbert, C., Guardiola, A., Shao, R., Kawaguchi, Y., Ito, A., Nixon, A., Yoshida, M., Wang, X.F., Yao, T.P., 2002. HDAC6 is a microtubule-associated deacetylase. Nature 417, 455–458.

Jensen, E.D., Gopalakrishnan, R., Westendorf, J.J., 2009. Bone morphogenic protein 2 activates protein kinase D to regulate histone deacetylase 7 localization and repression of Runx2. J. Biol. Chem. 284, 2225–2234.

Kalia, L.V., Lang, A.E., 2015. Parkinson's disease. Lancet 386, 896–912.

Kidd, S.K., Schneider, J.S., 2010. Protection of dopaminergic cells from MPP+-mediated toxicity by histone deacetylase inhibition. Brain Res. 1354, 172–178.

Kidd, S.K., Schneider, J.S., 2011. Protective effects of valproic acid on the nigrostriatal dopamine system in a 1-methyl-4-phenyl-1,2,3,6-tetrahydropyridine mouse model of Parkinson's disease. Neuroscience 194, 189–194.

Kontopoulos, E., Parvin, J.D., Feany, M.B., 2006. Alpha-synuclein acts in the nucleus to inhibit histone acetylation and promote neurotoxicity. Hum. Mol. Genet. 15, 3012–3023.

Kouroupi, G., Taoufik, E., Vlachos, I.S., Tsioras, K., Antoniou, N., Papastefanaki, F., Chroni-Tzartou, D., Wrasidlo, W., Bohl, D., Stellas, D., Politis, P.K., Vekrellis, K., Papadimitriou, D., Stefanis, L., Bregestovski, P., Hatzigeorgiou, A.G., Masliah, E., Matsas, R., 2017. Defective synaptic connectivity and axonal neuropathology in a human iPSC-based model of familial Parkinson's disease. Proc. Natl. Acad. Sci. U. S. A. 114, E3679–E3688.

Kurdistani, S.K., Grunstein, M., 2003. Histone acetylation and deacetylation in yeast. Nat. Rev. Mol. Cell Biol. 4, 276–284.

Labbe, C., Lorenzo-Betancor, O., Ross, O.A., 2016. Epigenetic regulation in Parkinson's disease. Acta Neuropathol. 132, 515–530.

Lang, C., Campbell, K.R., Ryan, B.J., Carling, P., Attar, M., Vowles, J., Perestenko, O.V., Bowden, R., Baig, F., Kasten, M., Hu, M.T., Cowley, S.A., Webber, C., Wade-Martins, R., 2019. Single-cell sequencing of iPSC-dopamine neurons reconstructs disease progression and identifies HDAC4 as a regulator of Parkinson cell phenotypes. Cell Stem Cell 24, 93–106 e106.

Lobera, M., Madauss, K.P., Pohlhaus, D.T., Wright, Q.G., Trocha, M., Schmidt, D.R., Baloglu, E., Trump, R.P., Head, M.S., Hofmann, G.A., Murray-Thompson, M., Schwartz, B., Chakravorty, S., Wu, Z., Mander, P.K., Kruidenier, L., Reid, R.A., Burkhart, W., Turunen, B.J., Rong, J.X., Wagner, C., Moyer, M.B., Wells, C., Hong, X., Moore, J.T., Williams, J.D., Soler, D., Ghosh, S., Nolan, M.A., 2013. Selective class IIa histone deacetylase inhibition via a nonchelating zinc-binding group. Nat. Chem. Biol. 9, 319–325.

Marek, L., Hamacher, A., Hansen, F.K., Kuna, K., Gohlke, H., Kassack, M.U., Kurz, T., 2013. Histone deacetylase (HDAC) inhibitors with a novel connecting unit linker region reveal a selectivity profile for HDAC4 and HDAC5 with improved activity against chemoresistant cancer cells. J. Med. Chem. 56, 427–436.

Mazzocchi, M., Wyatt, S.L., Mercatelli, D., Morari, M., Morales-Prieto, N., Collins, L.M., Sullivan, A.M., O'Keeffe, G.W., 2019. Gene co-expression analysis identifies histone deacetylase 5 and 9 expression in midbrain dopamine neurons and as regulators of neurite growth via bone morphogenetic protein signaling. Front. Cell Dev. Biol. 7, 191.

Mazzocchi, M., Collins, L.M., Sullivan, A.M., O'Keeffe, G.W., 2020. The class II histone deacetylases as therapeutic targets for Parkinson's disease. Neuronal Signal. 4, NS20200001.

O'Keeffe, G.W., Sullivan, A.M., 2018. Evidence for dopaminergic axonal degeneration as an early pathological process in Parkinson's disease. Parkinsonism Relat. Disord. 56, 9–15.

Paiva, I., Pinho, R., Pavlou, M.A., Hennion, M., Wales, P., Schutz, A.L., Rajput, A., Szego, E.M., Kerimoglu, C., Gerhardt, E., Rego, A.C., Fischer, A., Bonn, S., Outeiro, T.F., 2017. Sodium butyrate rescues dopaminergic cells from alpha-synuclein-induced transcriptional deregulation and DNA damage. Hum. Mol. Genet. 26, 2231–2246.

Pandey, U.B., Nie, Z., Batlevi, Y., McCray, B.A., Ritson, G.P., Nedelsky, N.B., Schwartz, S.L., DiProspero, N.A., Knight, M.A., Schuldiner, O., Padmanabhan, R., Hild, M., Berry, D.L., Garza, D., Hubbert, C.C., Yao, T.P., Baehrecke, E.H., Taylor, J.P., 2007. HDAC6 rescues neurodegeneration and provides an essential link between autophagy and the UPS. Nature 447, 859–863.

Park, G., Tan, J., Garcia, G., Kang, Y., Salvesen, G., Zhang, Z., 2016. Regulation of histone acetylation by autophagy in Parkinson disease. J. Biol. Chem. 291, 3531–3540.

Pinho, B.R., Reis, S.D., Guedes-Dias, P., Leitao-Rocha, A., Quintas, C., Valentao, P., Andrade, P.B., Santos, M.M., Oliveira, J.M., 2016. Pharmacological modulation of HDAC1 and HDAC6 in vivo in a zebrafish model: therapeutic implications for Parkinson's disease. Pharmacol. Res. 103, 328–339.

Poewe, W., Seppi, K., Tanner, C.M., Halliday, G.M., Brundin, P., Volkmann, J., Schrag, A.E., Lang, A.E., 2017. Parkinson disease. Nat. Rev. Dis. Primers. 3, 17013.

Rai, M., Soragni, E., Chou, C.J., Barnes, G., Jones, S., Rusche, J.R., Gottesfeld, J.M., Pandolfo, M., 2010. Two new pimelic diphenylamide HDAC inhibitors induce sustained frataxin upregulation in cells from Friedreich's ataxia patients and in a mouse model. PLoS One 5, e8825.

Ramasamy, A., Trabzuni, D., Guelfi, S., Varghese, V., Smith, C., Walker, R., De, T., Consortium, U.K.B.E., North American Brain Expression, C., Coin, L., de Silva, R., Cookson, M.R., Singleton, A.B., Hardy, J., Ryten, M., Weale, M.E., 2014. Genetic variability in the regulation of gene expression in ten regions of the human brain. Nat. Neurosci. 17, 1418–1428.

Rivieccio, M.A., Brochier, C., Willis, D.E., Walker, B.A., D'Annibale, M.A., McLaughlin, K., Siddiq, A., Kozikowski, A.P., Jaffrey, S.R., Twiss, J.L., Ratan, R.R., Langley, B., 2009. HDAC6 is a target for protection and regeneration following injury in the nervous system. Proc. Natl. Acad. Sci. U. S. A. 106, 19599–19604.

Rocha, E.M., De Miranda, B., Sanders, L.H., 2018. Alpha-synuclein: pathology, mitochondrial dysfunction and neuroinflammation in Parkinson's disease. Neurobiol. Dis. 109, 249–257.

Santo, L., Hideshima, T., Kung, A.L., Tseng, J.C., Tamang, D., Yang, M., Jarpe, M., van Duzer, J.H., Mazitschek, R., Ogier, W.C., Cirstea, D., Rodig, S., Eda, H., Scullen, T., Canavese, M., Bradner, J., Anderson, K.C., Jones, S.S., Raje, N., 2012. Preclinical activity, pharmacodynamic, and pharmacokinetic properties of a selective HDAC6 inhibitor, ACY-1215, in combination with bortezomib in multiple myeloma. Blood 119, 2579–2589.

Spillantini, M.G., Schmidt, M.L., Lee, V.M., Trojanowski, J.Q., Jakes, R., Goedert, M., 1997. Alpha-synuclein in Lewy bodies. Nature 388, 839–840.

Sugo, N., Oshiro, H., Takemura, M., Kobayashi, T., Kohno, Y., Uesaka, N., Song, W.J., Yamamoto, N., 2010. Nucleocytoplasmic translocation of HDAC9 regulates gene expression and dendritic growth in developing cortical neurons. Eur. J. Neurosci. 31, 1521–1532.

Taniguchi, M., Carreira, M.B., Cooper, Y.A., Bobadilla, A.C., Heinsbroek, J.A., Koike, N., Larson, E.B., Balmuth, E.A., Hughes, B.W., Penrod, R.D., Kumar, J., Smith, L.N., Guzman, D., Takahashi, J.S., Kim, T.K., Kalivas, P.W., Self, D.W., Lin, Y., Cowan, C.W., 2017. HDAC5 and its target gene, Npas4, function in the nucleus accumbens to regulate cocaine-conditioned behaviors. Neuron 96, 130–144 e136.

Tapia, M., Wandosell, F., Garrido, J.J., 2010. Impaired function of HDAC6 slows down axonal growth and interferes with axon initial segment development. PLoS One 5, e12908.

Thaler, F., Mercurio, C., 2014. Towards selective inhibition of histone deacetylase isoforms: what has been achieved, where we are and what will be next. ChemMedChem 9, 523–526.

Trazzi, S., Fuchs, C., Viggiano, R., De Franceschi, M., Valli, E., Jedynak, P., Hansen, F.K., Perini, G., Rimondini, R., Kurz, T., Bartesaghi, R., Ciani, E., 2016. HDAC4: a key factor underlying brain developmental alterations in CDKL5 disorder. Hum. Mol. Genet. 25, 3887–3907.

van Heesbeen, H.J., Smidt, M.P., 2019. Entanglement of genetics and epigenetics in Parkinson's disease. Front. Neurosci. 13, 277.

Wang, Y., Wang, X., Liu, L., Wang, X., 2009. HDAC inhibitor trichostatin A-inhibited survival of dopaminergic neuronal cells. Neurosci. Lett. 467, 212–216.

Wu, Q., Yang, X., Zhang, L., Zhang, Y., Feng, L., 2017. Nuclear accumulation of histone deacetylase 4 (HDAC4) exerts neurotoxicity in models of Parkinson's disease. Mol. Neurobiol. 54, 6970–6983.

Xicoy, H., Wieringa, B., Martens, G.J., 2017. The SH-SY5Y cell line in Parkinson's disease research: a systematic review. Mol. Neurodegener. 12 (1), 10. https://doi.org/10.1186/s13024-017-0149-0.

Yang, X.J., Seto, E., 2007. HATs and HDACs: from structure, function and regulation to novel strategies for therapy and prevention. Oncogene 26, 5310–5318.

Yu, P.B., Hong, C.C., Sachidanandan, C., Babitt, J.L., Deng, D.Y., Hoyng, S.A., Lin, H.Y., Bloch, K.D., Peterson, R.T., 2008. Dorsomorphin inhibits BMP signals required for embryogenesis and iron metabolism. Nat. Chem. Biol. 4, 33–41.